Chemical Engineering Science 308 (2025) 121416

Contents lists available at ScienceDirect

Chemical Engineering Science

journal homepage: www.elsevier.com/locate/ces

A simplified CFD approach for modeling mass transport in catalytic open-cell foams

Ginu R. George [a], Sai Krishna Danda [b], Gregor D. Wehinger [c,*]

[a] Oak Ridge National Laboratory, 1 Bethel Valley Road, Oak Ridge, TN 37830, USA
[b] CASCATE GmbH, Industriestr. 2, 70565 Stuttgart, Germany
[c] Institute of Chemical Process Engineering, Karlsruhe Institute of Technology, Kaiserstr. 12, 76131 Karlsruhe, Germany

ARTICLE INFO

Keywords:
Open-cell foam
CFD
Mass transport
CO oxidation
Heterogeneous catalysis

ABSTRACT

A simplified macroscopic CFD approach is presented to model mass transport including chemical reactions in washcoated open-cell foams. The foam is treated as a porous medium. Species conversion during chemical reactions is modeled using appropriate source terms based on reaction rate expressions and modified to account for the mass transport resistances occurring at the fluid-washcoat interfaces and within the washcoat layers. As example, the catalytic CO oxidation over platinum is studied. The simulation results show good agreement with experimental data from literature. A parametric study on washcoat parameters, such as thickness, tortuosity, porosity, and size, is carried out. Increasing the washcoat thickness from 5 to 100 μm or decreasing the tortuosity to porosity ratio from 5 to 20 decreases the CO conversion by 10 %. The proposed model is found to be reliable and has the advantage of lower computational cost, making it a suitable tool for foam-based catalytic reactor design.

1. Introduction

Open-cell foams are multifunctional materials, used in many engineering applications (Wan et al., 2021; Ozmat et al., 2004; Bird et al., 2018; Napolitano et al., 2017). Among them, a great deal of interest can be found in the use of ceramic and metal foams as catalyst supports for heterogeneous catalytic reactions (Makhania and Upadhyayula, 2022; Ho et al., 2019; Twigg and Richardson, 2007). Since foams possess superior properties of high porosity (75–95 %) and high specific surface area, they provide efficient mass transfer combined with a lower pressure drop in comparison to conventional packed beds (Patcas et al., 2007; Papetti et al., 2018). In recent times, pelletized catalysts have also been made from alloyed metallic foams, and identified as promising in tubular reactors (Walther et al., 2008; Kim and Lee, 2014; George et al., 2023).

A common method for chemically activating the foam substrate is by washcoating, in which the catalytic active sites are dispersed within the washcoat layer (Makhania and Upadhyayula, 2022). The reactants diffuse into the porous washcoat and react on active catalyst sites, along with the release or intake of heat, i.e., exothermic or endothermic reactions. The tortuous flow path induced by the foam geometry and the accompanied convection–diffusion-reaction mechanisms for mass transfer are rather complex to analyze. The transport characteristics of open-cell foams have been experimentally investigated by many authors and suitable correlations have been reported extensively for pressure drop (Kumar and Topin, 2017; Lacroix et al., 2007; Inayat, 2013; Inayat et al., 2016; Edouard et al., 2008) and heat transfer (Giani et al., 2005; Manetti et al., 2022; Lu et al., 1998; Wang et al., 2020; Zhao, 2012), while mass transfer studies are rather limited (Giani et al., 2005; Groppi et al., 2007; Incera Garrido et al., 2008; Incera Garrido and Kraushaar-Czarnetzki, 2010; Bracconi et al., 2018).

Mass transport in open-cell foams has also been investigated numerically, via Computational Fluid Dynamics (CFD), with different levels of detail on foam geometry and chemical reaction modeling. Dong et al. (Dong et al., 2018) have conducted strut-resolved CFD simulations for the oxidation of carbon monoxide in a Pt-coated foam monolith, and validated with their own experimental data. They used X-ray microtomography to create a realistic foam geometry, and the catalytic chemistry was modeled by a microkinetic reaction model. Although the microkinetic model is the most detailed approach that considers elementary reaction steps on the catalytic surface, the coupling of microkinetics to the CFD framework is very challenging and computationally expensive, mainly due to the stiffness and non-linearity of the corresponding equations to be solved (Maestri and Cuoci, 2013; Daymo et al., 2022). Della Torre et al. (Della Torre et al., 2016) have

* Corresponding author.
E-mail address: gregor.wehinger@kit.edu (G.D. Wehinger).

https://doi.org/10.1016/j.ces.2025.121416
Received 30 September 2024; Received in revised form 23 January 2025; Accepted 22 February 2025
Available online 24 February 2025

Nomenclature

Latin symbols:

a	pore size (m)
a_v	interfacial area per unit volume (m^{-1})
C_s	fluid-washcoat Interfacial concentration (mol m^{-3})
C_{fm}	cup-mixing concentration (bulk fluid phase) (mol m^{-3})
C_{wc}	volume averaged concentration inside washcoat (mol m^{-3})
$D_{e,i}$	effective diffusion coefficient of component i (m^2 s^{-1})
$D_{knud,\,i}$	Knudsen diffusion coefficient of component i (m^2 s^{-1})
d_s	strut diameter (m)
k_{me}	external mass transport coefficient (m s^{-1})
k_{mi}	internal mass transport coefficient (m s^{-1})
k_{mo}	overall mass transport coefficient (m s^{-1})
$k_{R,\,i}$	intrinsic reaction rate constant of component i (s^{-1})
$k_{app,i}$	apparent rate constant (s^{-1})
l_D	diffusion length or shape factor (m)
l_{foam}	characteristic length scale of foam structure
l_{wc}	characteristic length scale of washcoat
NR	number of reactions
P	order of the reaction
r_j	reaction rate (mol g.cat^{-1} s^{-1})
v_s	superficial velocity of fluid (m s-1)

Greek symbols:

α_{ij}	Stoichiometry coefficient of species i in reaction j
ϵ_{foam}	foam porosity
Γ	Thiele modulus
λ_{eff}	effective foam thermal conductivity
$\lambda_{foam,b}$	bulk foam thermal conductivity
λ_f	fluid thermal conductivity

Dimensionless numbers:

$Re_{foam} = \rho_f v_s l_{foam}/\mu_f$ foam Reynolds number

$Sh_e = \frac{k_{me} l_{foam}}{D_f}$ external Sherwood number

$Sh_i = \frac{k_{mi} l_{wc}}{D_e}$ internal Sherwood number

$Sh_{i,\,\infty}$ asymptotic internal Sherwood number

implemented a CFD model based on a coupled finite-volume and finite-area method to describe mass transfer phenomena occurring in the fluid phase and over the surface of catalytic open-cell foams. The foam geometry was approximated by arranging a series of regular Kelvin cells in a row, and the catalytic combustion of CO was considered by a kinetic model of Langmuir-Hinshelwood type. Wehinger et al. (Wehinger et al., 2016) have presented an automated workflow for a detailed CFD simulation of open-cell foams. The foam structure was generated by a foam modeler based on Voronoi tessellations. They also illustrated the partial oxidation of methane in a foam monolith coated with rhodium catalyst by applying a microkinetic reaction mechanism, but without considering diffusion processes in the washcoat. Even though different CFD approaches for modeling mass transport phenomena in open-cell foams have been presented, a method suitable for a randomly packed bed composed of hundreds or thousands of foam pellets is lacking. In this context, a much simpler approach compromising the computational cost is necessary to deal with the great number of foam pellets. In addition, a reliable approach should consider mass transport limitations, particularly the washcoat diffusion resistance (von Rickenbach et al., 2015; Makhania and Upadhyayula, 2022; Aguirre et al., 2020), which is, however, ignored in most of the studies.

In this work, a macroscopic CFD approach is used to model the mass transport in a catalytic washcoated open-cell foam. This paper extends our previous work (George et al., 2021; George et al., 2022); where we have presented methods to model the flow and the energy transport inside foam pellets, for use in fixed-bed reactors. In this contribution, the catalytic foam is modeled macroscopically as a porous medium, in which the production and consumption of species during catalytic reactions are considered by appropriate source or sink terms, supported by relevant kinetic models of Langmuir-Hinshelwood type. To account for mass transport limitations, the concept of external and internal mass transport coefficients, proposed by Joshi et al. (Joshi et al., 2009), is adopted. For illustration, the oxidation of carbon monoxide on a platinum supported foam monolith is simulated using the macroscopic CFD approach. The results are validated with experimental data available in literature (Dong et al., 2018). Furthermore, a parametric study is conducted to quantify the influence of different washcoat parameters, such as thickness, tortuosity, porosity, and pore diameter, on the reactor performance.

2. Material and methods

2.1. Modeling mass transport

A macroscopic approach to model the flow and energy transport inside open-cell foam pellets was presented in prior work (George et al., 2021; George et al., 2022). The proposed framework was based on the porous-media approach, where the inner foam structures such as struts, knots, and pores were not resolved, but rather dependent on the appropriate sub-models to account for pressure loss and thermal transport within foam pellets. Adhering to this porous-media approach, a simplified method for simulating mass transport including chemical reactions in a washcoated foams is discussed in the following sections.

2.1.1. External and internal mass transport limitations

Since the open-cell foams are highly porous, the reactants have direct access by convection and diffusion to the washcoated struts on which the catalyst is deposited (see Fig. 1 (A-B)). When reactants diffuse into the porous washcoat, they undergo reactions, and the products formed diffuse back to the fluid phase. The actual processing conditions, however, impose different limitations on such transport phenomena (Fogler, 2020). By the classical approach, the resistances to mass transfer can be evaluated with the concept of transport coefficients, which are generally defined upon the assumption that the entire resistance resides in a hypothetical stagnant film within which the concentration variation occurs (Incropera et al., 2007). Following this method, Joshi et al. (Joshi et al., 2009; Joshi et al., 2009) have presented a two-film resistance model for catalytic monoliths, which accounts for transport resistances in the gas phase and solid phase (washcoat layer). Considering the similarity in underlying mechanisms, mainly at the fluid-washcoat interface, the same method for structured monoliths is applicable to catalytic foams, as adapted in ref. (Moncada Quintero et al., 2021).

Fig. 1 (C) illustrates the mass transport resistances in a catalytic foam. The resistance for mass transfer in the gas phase resides in a thin film along the fluid-washcoat interface, where the concentration drops from the cup-mixing concentration C_{fm} to fluid-washcoat interfacial concentration C_s. In this region, external mass transfer occurs, and the corresponding external transport coefficient is k_{me}. Similarly, the resistance to internal diffusion in the washcoat region is described by a narrow fictitious washcoat zone, where the interfacial concentration C_s drops to concentration C_{wc} inside the washcoat. C_{wc} is a volume averaged concentration and assumed to be constant in the bulk of the washcoat. This internal mass transport can be represented by the

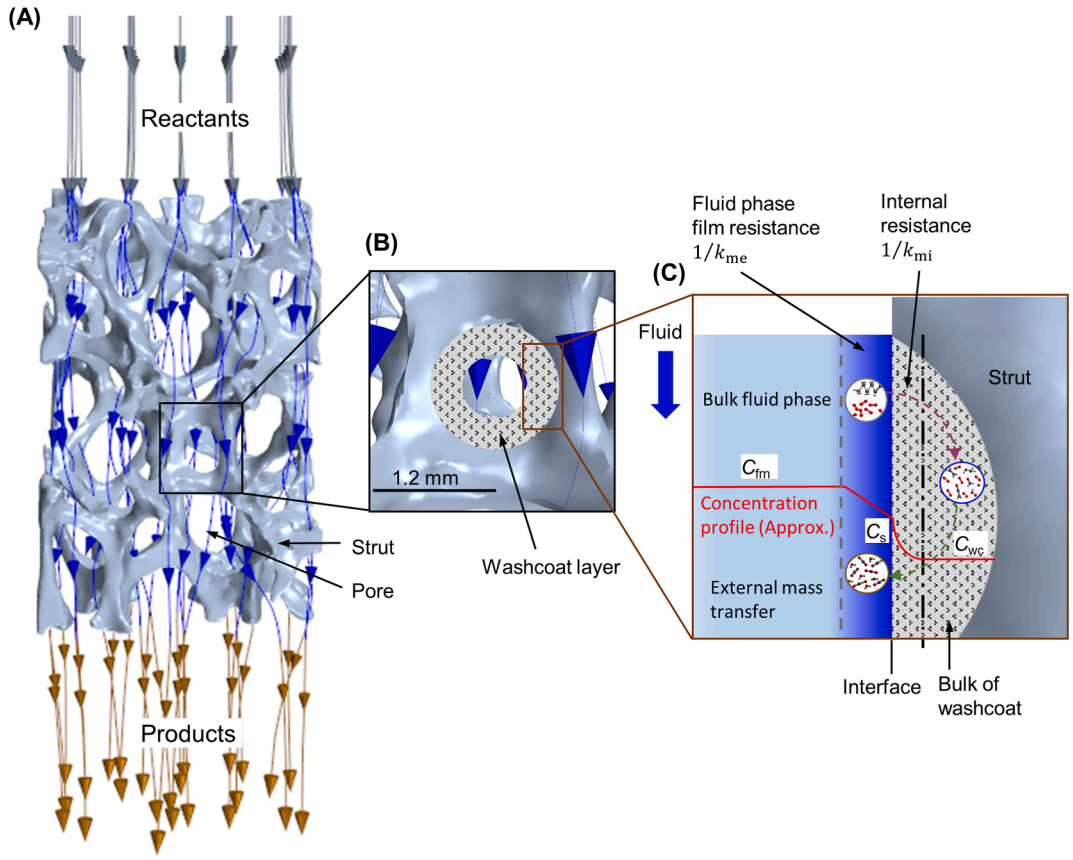

Fig. 1. (A) Flow streamlines through a foam structure; Illustration of (B) washcoated foam strut, and (C) mass transport resistances.

internal mass transport coefficient k_{mi}.

As there is no accumulation of mass at the fluid-washcoat interface, the external and internal transport coefficients can be related to mass transfer rate $\dot{n}$ as (Joshi et al., 2009):

$$\dot{n} = k_{me}(C_{fm} - C_s) = k_{mi}(C_s - C_{wc}) \quad (1)$$

When there are several resistances to mass transfer, the total mass flux is always proportional to the overall resistance. Accordingly, an overall mass transfer coefficient for the catalytic foam can be defined as (Joshi et al., 2009):

$$\frac{1}{k_{mo}} = \frac{1}{k_{me}} + \frac{1}{k_{mi}} \quad (2)$$

Several studies have been conducted on the external mass transfer coefficient of open-cell foams. Correlations for estimating k_{me} based on foam structural parameters have been presented in refs. (Giani et al., 2005; Groppi et al., 2007; Incera Garrido et al., 2008; Incera Garrido and Kraushaar-Czarnetzki, 2010; Bracconi et al., 2018). In this work, the correlation proposed by Incera Garrido et al. (Incera Garrido et al., 2008); Eqs. (3–4), are used to determine k_{me}.

$$Sh_e = 1.0 \bullet Re_{foam} \bullet Sc^{1/3} \bullet F_g \quad (3)$$

$$k_{me} = \frac{Sh_e D_f}{l_{foam}} \quad (4)$$

Here, Sh_e is the external Sherwood number, which relates the convective and diffusive mass fluxes at the fluid-strut interface; $Re_{foam} = \rho_f v_s l_{foam}/\mu_f$ is the foam Reynolds number based on the characteristic length $l_{foam} = a + d_s$, with pore size a and strut diameter d_s; v_s is the superficial velocity of fluid with density ρ_f and dynamic viscosity μ_f; $Sc = \mu_f/\rho_f D_f$ is the Schmidt number and D_f is the molecular diffusivity in the fluid phase; $F_g = \left(l_{foam}[m]/0.001[m]\right)^{0.58} \bullet \varepsilon_{foam}^{0.44}$ is the foam geometrical parameter relating foam porosity ε_{foam}. It should be noted that [m] in the equation of F_g denotes the unit meter, see (Incera Garrido et al., 2008) for the detailed formulation of Eq. (3).

To estimate the internal mass transfer coefficient k_{mi}, the correlation, Eqs. (5–6), proposed by Joshi et al. (Joshi et al., 2009) is used.

$$Sh_i = Sh_{i\infty} + \frac{\zeta \Gamma^2}{1+\zeta\Gamma} \quad (5)$$

$$k_{mi} = \frac{Sh_i D_e}{l_{wc}} \quad (6)$$

where: Sh_i is the internal Sherwood number; $Sh_{i\infty}$ is the asymptotic internal Sherwood number obtained in the limit of a slow reaction; ζ is a constant, dependent on washcoat geometry and kinetic parameters; Γ is the Thiele modulus; l_{wc} is the characteristic length scale for washcoat and it is defined as the ratio of washcoat cross-sectional area to the interfacial perimeter. Joshi et al. (Joshi et al., 2009; Joshi et al., 2009) have provided the numerically computed values of $Sh_{i\infty}$ and ζ for different washcoat geometries. Table 1 lists $Sh_{i\infty}$; ζ and l_{wc} of selected washcoat shapes which are considered in this work. The washcoat shape represents the cross-sectional profile of a washcoated channel, assuming it remains constant along the channel length. In this study, circular (or annular) and hexagonal washcoated channels were considered, with the assumption that both shapes have the same circular flow area. In the circular channel, the washcoat thickness is uniform around the circumference, whereas in the hexagonal shape, the thickness varies at the corners, similar to other commonly used washcoated channel geometries such as square and triangle. In actual foam structures, there is a greater chance of more washcoat being deposited at the strut joints.

A generalized equation of the Thiele modulus Γ for a reaction with an order p is given by (Roy et al., 2004):

$$\Gamma = l_D \sqrt{\frac{p+1}{2}} \sqrt{\frac{k_R C_{fm}^{p-1}}{D_e}} \quad (7)$$

For washcoated foams, the diffusion length or shape factor $l_D = l_{wc}$ (Joshi et al., 2009; Moncada Quintero et al., 2021). D_e is the effective diffusivity of the reactant in the washcoat, and k_R is the average reactivity. Assuming a first-order kinetics, Eq. (7) can be simplified as (Joshi et al., 2009):

$$\Gamma^2 = \frac{k_R l_{wc}^2}{D_e} \quad (8)$$

The effective diffusion coefficient of species i in the washcoat is given

Table 1
Characteristic length scale l_{wc}, asymptotic internal Sherwood number $Sh_{i\infty}$, and shape constant ζ for different washcoat shapes (from refs. (Joshi et al., 2009; Joshi et al., 2009).

Washcoat shape	l_{wc}	$Sh_{i\infty}$ and ζ		
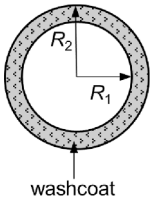	$(R_2^2 - R_1^2)/(2R_1)$	R_2/R_1	$Sh_{i\infty}$	ζ
		1.01	3.013	0.38
		1.1	3.153	0.36
		1.2	3.311	0.34
		1.5	3.818	0.27#
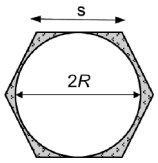	$(3\sqrt{3}s^2 - 2\pi R^2)/(4\pi R)$	s/R	$Sh_{i\infty}$	ζ
		1.155	0.814	0.77
		1.17	1.16	2.08
		1.2	1.74	1.60

Value obtained by extrapolation.

by (von Rickenbach et al., 2015):

$$\frac{1}{D_{e,i}} = \frac{\tau_{wc}}{\varepsilon_{wc}}\left(\frac{1}{D_{knud,i}} + \frac{1}{D_i}\right) \quad (9).$$

where, τ_{wc} and ε_{wc} are the washcoat tortuosity and porosity, respectively. The Knudsen diffusion coefficient $D_{knud,i}$ is determined by using an average washcoat pore diameter d_{wc} and the species molecular weight M_i as (von Rickenbach et al., 2015):

$$D_{knud,i} = \frac{d_{wc}}{3}\sqrt{\frac{8RT}{\pi M_i}} \quad (10).$$

Makhania and Upadhyayula (Makhania and Upadhyayula, 2022) have stated that the tortuous foam geometry stimulates the diffusion of species into the washcoat, which should also be considered in determining D_e. They used the foam tortuosity τ_{foam} instead of washcoat tortuosity τ_{wc} to estimate D_e, and calculated the Thiele modulus and effectiveness factor, resulted a better agreement between theoretical equations and detailed simulations.

Accordingly, Eq. (9) to determine $D_{e,i}$ is modified to account for the influence of foam tortuosity τ_{foam} and foam porosity ε_{foam} as:

$$\frac{1}{D_{e,i}} = \frac{\tau_{wc}}{\varepsilon_{wc}}\left(\frac{1}{D_{knud,i}}\right) + \frac{\tau_{foam}}{\varepsilon_{foam}}\left(\frac{1}{D_i}\right) \quad (11).$$

The tortuosity of an open-cell foam can be estimated by (Inayat et al., 2016):

$$\tau_{foam} = 1 + \varnothing\frac{\left[1-0.971\left(1-\varepsilon_{foam}\right)^{0.5}\right]}{4\varepsilon_{foam}\left(1-\varepsilon_{foam}\right)^{0.5}}\left(1-\varepsilon_{foam}\right) \quad (12).$$

where, $\varnothing$ is the strut shape factor; for the cylindrical strut $\varnothing \approx 4.87$ (Inayat et al., 2016).

The concept of the internal Sherwood number and its formulation have been explained in detail in refs. (Joshi et al., 2009; Joshi et al., 2009; Balakotaiah, 2008; Bhattacharya et al., 2004).

2.1.2. Apparent reaction rate

To determine the apparent reaction rate, the intrinsic reaction rate should be adapted with mass transfer resistances. In modeling foam based catalyst converters, Hayes et al. (Hayes et al., 2012) have presented a method to derive the apparent reaction rate. The same method was followed in this study.

Considering $k_{R,i}$ as the intrinsic reaction rate, the average reaction rate $\overline{R}_i$ of species i in terms of mass fraction in the washcoat $Y_{i,wc}$ is:

$$\overline{R}_i = k_{R,i}\rho_f Y_{i,wc} \quad (13).$$

The total mass transfer into the bulk fluid phase and the bulk reaction rate in the washcoat can be related as:

$$\dot{m} = k_{mo}a_v\rho_f\left(Y_{i,fm} - Y_{i,wc}\right) = \beta k_{R,i}\rho_s Y_{i,wc} \quad (14).$$

where, k_{mo} is the overall mass transport coefficient as per Eq. (2), $Y_{i,fm}$ is the mass fraction of species i in the bulk phase (see Fig. 1 (C)). The washcoat factor β accounts for the reduced availability and accessibility of active catalyst particles relative to entire geometric surface area – a correction factor which could take values between 1 and 0. The interfacial area per unit volume a_v is assumed to be equal to the specific geometric surface area of the foam catalyst, estimated by an empirical model (Incera Garrido et al., 2008):

$$a_v = 3.84\left(l_{foam}\right)^{-0.85}\varepsilon_{foam}^{-0.82} \quad (15)$$

$l_{foam} = a + d_s$, with pore size a and strut diameter d_s.

On rearranging Eq. (14), a relationship between the mass fraction in the bulk fluid phase and bulk washcoat can be obtained as:

$$Y_{i,wc} = \left(\frac{k_{mo}a_v\rho_f}{\beta k_{R,i}\rho_s + k_{mo}a_v\rho_f}\right)Y_{i,fm} \quad (16)$$

Substituting Eq. (16) into Eq. (13) yields the apparent average reaction rate of species i in the washcoat:

$$\overline{R}_{i,app} = \underbrace{k_{R,i}\left(\frac{k_{mo}a_v\rho_f}{\beta k_{R,i}\rho_s + k_{mo}a_v\rho_f}\right)}_{k_{app,i}}\rho_f Y_{i,fm} = k_{app,i}\rho_f Y_{i,fm} \quad (17)$$

The apparent rate constant $k_{app,i}$ can be written as:

$$\frac{1}{k_{app,i}} = \frac{1}{\beta k_{R,i}} + \frac{\rho_s}{k_{mo}a_v\rho_f} \quad (18)$$

For heterogeneous catalytic surface reactions, the intrinsic kinetics can be determined experimentally, and the intrinsic rate equations or models can be derived, primarily by using the Langmuir-Hinshelwood-Hougen-Watson (LHHW) approach (Hou and Hughes, 2001; Batebi et al., 2021; Barteau et al., 1981). A common form to calculate the intrinsic rate constant of species i; $k_{R,i}$ in [s^{-1}] is:

$$k_{R,i} = \sum_{j=1}^{NR}\left(\alpha_{ij}r_j\right)M_i \quad (19)$$

where: NR is the number of reactions, α_{ij} is the stoichiometry coefficient of species i in the reaction j, r_j is the reaction rate in [mol g.cat^{-1} s^{-1}], M_i is the molecular weight of species i in [g mol^{-1}].

Using Eq. (18), $k_{R,i}$ obtained from kinetic models can be modified to $k_{app,i}$, which includes the effect of mass transfer resistances. Accordingly, an apparent source or sink term for the production or consumption of species i upon chemical reactions in a catalytic foam of density ρ_s is given by:

$$S_{i,app} = \rho_s k_{app,i}Y_{i,wc} \quad (20)$$

2.2. Illustrative example

For the illustration of the mass transport modeling approach mentioned above, the oxidation of carbon monoxide in a Pt-coated foam catalyst monolith, provided by Dong et al. (Dong et al., 2018), was chosen. The authors have measured the axial species concentration and temperature profiles along the center core of a foam monolith under CO oxidation on Pt nanoparticles. The Pt-coated α-Al_2O_3 foam catalyst, with a length of 20.1 mm, was inserted into a silica reactor tube having an inner diameter of 18 mm. At the center core of the foam, a small channel of about 1 mm was drilled to place a sampling capillary of about 700 μm outer diameter, which has a sampling orifice of about 100 μm. Dong et al. (Dong et al., 2018) have also conducted strut-resolved CFD simulations, in which the foam structure was digitalized by X-ray microtomography and the catalytic chemistry was modeled by a microkinetic reaction model of Deutschmann et al. (Deutschmann et al., 1996). A detailed description on experimental setup, measuring procedures, and numerical study can be found in the refs. (Dong et al., 2018; Korup et al., 2011).

In accordance with the experimental reactor, a setup for macroscopic

CFD simulations was realized as shown in Fig. 2 (A). The CFD domain was composed of a porous region representing the catalytic foam, and a fluid region for the extended outlet section. The meshing was carried out using Siemens Simcenter STAR-CCM + version 16.06, with polyhedral cells in the bulk region and prism-layer cells at wall-boundary regions, see Fig. 2 (B) The total cell count was about 30,000. At the inlet, uniform velocity and temperature were assumed. No-slip wall boundary condition was assigned to the reactor tube wall, foam surface and capillary wall. The capillary wall were set as adiabatic, and a constant heat loss of 20 W was assigned across the reactor wall, in accordance with the observations in ref. (Dong et al., 2018). A pressure boundary condition was assigned at the outlet of the simulation domain. Table 2 lists the inlet gas composition and other boundary values. The relevant properties of the foam and the washcoat are provided in Table 3.

The flow condition was assumed to be laminar, and simulations were carried out at steady-state upon solving the governing equations by the finite-volume method, using Siemens Simcenter STAR-CCM + version 16.06. A detailed description on fundamental equations can be found elsewhere (Ferziger and Perić, 2002; Versteeg et al., 2007). The transport equations relevant to the porous domain (foam catalyst) are briefly discussed (Siemens Digital Industries Software, 2020).

Continuity equation:

$$\oint_A \varepsilon_{\text{foam}} \rho \mathbf{v} \cdot d\mathbf{a} = 0 \quad (21)$$

where: $\mathbf{v}$ is the physical or true velocity in the porous medium with porosity $\varepsilon_{\text{foam}}$, $\mathbf{a}$ is the area vector.

Momentum equation:

$$\oint_A \varepsilon_{\text{foam}} \rho \mathbf{v} \otimes \mathbf{v} \cdot d\mathbf{a} = -\oint_A \varepsilon_{\text{foam}} p\mathbf{I} \cdot d\mathbf{a} + \oint_A \varepsilon_{\text{foam}} \mathbf{T} \cdot d\mathbf{a} + \int_V \varepsilon_{\text{foam}} \mathbf{f}_b dV + \int_V \varepsilon_{\text{foam}} \mathbf{f}_p dV \quad (22)$$

where: $\otimes$ denotes the outer product, p is pressure, $\mathbf{T}$ is the viscous stress tensor, $\mathbf{I}$ is the Identity tensor, $\mathbf{f}_b$ is the resultant of body forces.

Table 2
Simulation parameters (from ref. (Dong et al., 2018)).

Feed compositions (in mole fraction):	
CO	0.126
O_2	0.063
CO_2	0.010
Ar	0.736
He	0.065
Inlet velocity [m s^{-1}]	0.341
Inlet temperature [K]	1490
Reference pressure [bar]	1
Wall heat loss [W]	20

Table 3
Properties of foam and washcoat (from refs. (Dong et al., 2018; von Rickenbach et al., 2015)).

Foam parameters:	
Cell size, ϕ [mm]	1.35 ± 0.09
Pore size, a [mm]	0.65 ± 0.09
Strut size, d_s [mm]	0.35 ± 0.09
Porosity,$\varepsilon_{\text{foam}}$	0.73 ± 0.02
Washcoat parameters (base case):	
Porosity,ε_{wc}	0.35
Tortuosity,τ_{wc}	3.5
Pore diameter,d_{wc} [nm]	10
Thickness [μm]	5
Washcoat shape	Annulus

The porous resistance $\mathbf{f}_p = \mathbf{P} \cdot \mathbf{v}_s$, with the resistance tensor $\mathbf{P} = \mathbf{P}_v + \mathbf{P}_i|\mathbf{v}_s|$. The viscous resistance tensor $\mathbf{P}_v$ and the inertial resistance tensor $\mathbf{P}_i$ were defined by the Lacroix correlation (Lacroix et al., 2007); Eqs.

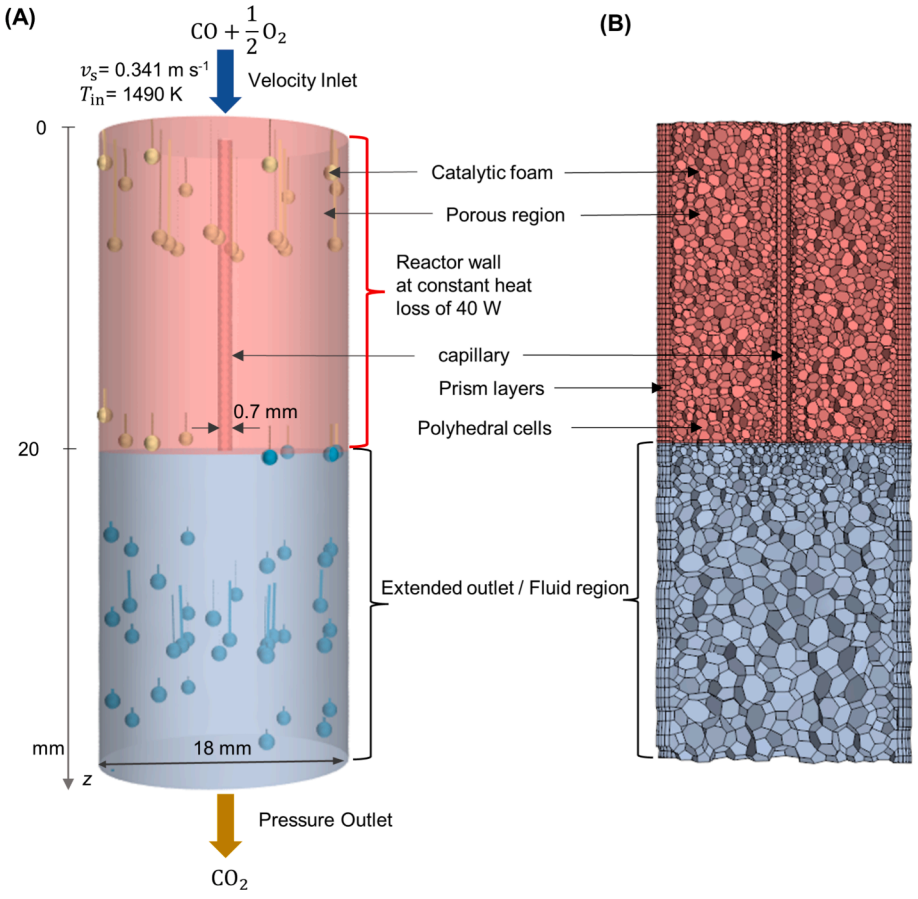

Fig. 2. (A) Simulation setup and boundary conditions; (B) Mesh details illustrated on a vertical slice.

(23, 24), based on the foam structural parameters such as cell size ϕ, pore size a, strut diameter d_s, and porosity $\varepsilon_{\text{foam}}$, see (George et al., 2021) for details and validation. The superficial velocity $\mathbf{v}_s$ is related to the true velocity as $\mathbf{v}_s = \varepsilon_{\text{foam}}\mathbf{v}$.

$$\frac{\nabla p}{L} = \mathrm{A}\frac{(1-\varepsilon)^2\mu}{\varepsilon^3(1.5d_s)^2}v_s + \mathrm{B}\frac{(1-\varepsilon)\rho}{\varepsilon^3(1.5d_s)}v_s^2 \quad (23)$$

$$d_s = \frac{a\left[\left(\frac{4}{3\pi}\right)(1-\varepsilon)\right]^{\frac{1}{2}}}{1-a\left[\left(\frac{4}{3\pi}\right)(1-\varepsilon)\right]^{\frac{1}{2}}} \quad (24)$$

Energy equation:

Based on the concept of thermal equilibrium in a porous domain ($T_{\text{fluid}} = T_{\text{solid}}$), the energy equation is given by:

$$\oint_A \varepsilon_{\text{foam}}\rho_{\text{fluid}} H_{\text{fluid}}\,\mathbf{v}\cdot d\mathbf{a} = \oint_A \lambda_{\text{eff}}\nabla T_{\text{fluid}}\cdot d\mathbf{a} + \oint_A \varepsilon_{\text{foam}}\mathbf{T}\cdot\mathbf{v}\cdot d\mathbf{a} + \int_V \varepsilon_{\text{foam}}\mathbf{f}_b\cdot\mathbf{v}dV + \int_V S_u^e dV \quad (25)$$

where: H_{fluid} is total enthalpy of fluid, S_u^e is energy source term. According to Schuetz and Glicksman (Schuetz and Glicksman, 1984), the effective foam thermal conductivity λ_{eff} is given by:

$$\lambda_{\text{eff}} = \varepsilon_{\text{foam}}\lambda_f + (1-\varepsilon_{\text{foam}})\tfrac{1}{3}\lambda_{\text{foam,b}} \quad (26)$$

where: λ_f is fluid conductivity and $\lambda_{\text{foam,b}}$ is bulk foam conductivity, see (George et al., 2022) for a detailed explanation.

The amount of heat released or consumed during a catalytic reaction is defined in the energy source term as (Karthik and Buwa, 2017; Dixon et al., 2012):

$$S_u^e = \rho_s\sum_{j=1}^{\text{NR}} r_j\left(-\Delta H_j\right) \quad (27)$$

where: ρ_s is the density of the foam; r_j and ΔH_j are the reaction rate and the heat of reaction for reaction j, respectively, and NR is the number of reactions.

Conservation of species i:

$$\oint_A (\rho Y_i\mathbf{v})\cdot d\mathbf{a} = \oint_A J_i\cdot d\mathbf{a} + \int_V S_{i,\text{app}}dV \quad (28)$$

where, $Y_i = m_i/m$ is the mass fraction of species i with mass m_i and total mixture mass m. The molecular diffusive flux J_i based on mixture-average formulation and for a porous medium is:

$$J_i = \rho_f\frac{\varepsilon_{\text{foam}}}{\tau_{\text{foam}}}\sum_{j=1}^{N} D_{i,j}\nabla Y_j \quad (29)$$

where: ρ_f is the fluid or mixture density and tortuosity of the foam, $D_{i,j}$ is the multi-component diffusion coefficient for species i and component j.

To determine the apparent source term $S_{i,\text{app}}$ (Eq. (20)) and heat source S_u^e (Eq. (27)) for the oxidation reaction of CO on supported platinum, the kinetic rate expression from Shishu and Kowalczyk (Shishu and Kowalczyk, 1974) was used. The kinetic parameters for the rate equation Eq. (30) is provided in Table 4, where p_i is the partial pressure of species i.

$$r = \frac{kK_{\text{CO}}K_{\text{O}_2}p_{\text{CO}}p_{\text{O}_2}}{\left(1+K_{\text{CO}}p_{\text{CO}}+K_{\text{O}_2}p_{\text{O}_2}\right)^2} \quad (30)$$

3. Results and discussion

3.1. Comparison of experiment and simulation

The simulation results have been verified with experimental data provided by Dong et al. (Dong et al., 2018). Fig. 3 (A) shows the comparison of species mole fractions at the center core of the catalytic foam along the axial direction. For the validation purpose, the washcoat properties presented in Table 3 are used, and the shape of the washcoat is assumed to be an annulus, with an outer-to-inner annulus ring ratio of R_2/R_1 1.01, see Table 1.

The species profiles predicted by CFD are in good agreement with experimental data, except at the reactor entry region ($0 < z^* < 0.2$). There may be many reasons for this discrepancy. In the Supporting Information, some of the possible reasons are discussed in detail. One of the possible reasons may be the discrepancies in the used kinetic model. The reaction rate and the resulting species profiles are strongly dependent on the kinetic parameters used. Since the modeled chemistry appears faster compared with experimentally determined species profiles, additional simulations were carried out by varying the pre-exponential factor in the rate equation (the original value is $1.4\cdot10^6$, see Table 4). Fig. 3 (A) also shows the CO_2 profiles for the modified pre-exponential factors of $1.0\cdot10^6$ and $0.8\cdot10^6$. As expected, the reaction rate decreases with the reduced pre-exponential factors. Other possibilities for the mismatch include – influence of local variations in the foam internal structure, i.e., pores and struts, and hence variation of local velocity and associated heat and mass transfer; difference in the catalyst composition in the washcoat, including the availability and accessibility of active Pt nanoparticles; simplified heat loss assumption; slight mismatch in flow conditions (velocity, temperature) upstream the catalytic foam inlet compared to the experiments, where inert foams were used, see (Dong et al., 2018). A discussion of the potential reasons for the mismatch between the experiment and simulation is presented in the Supplementary Information.

Fig. 3 (B) depicts the comparison of the center-line temperature profile. The simulated temperature profile is marginally higher than the measured. By adjusting the pre-exponential factors, the temperature profile slightly shifts to the lower side, due to the reduction in the amount of heat generated. It should also be highlighted that experimental artifacts are reported in the original work, which led to the peak temperature occurring directly at the catalytic foam entrance, see (Dong et al., 2018) and Supplementary Information for details. Since the catalytic reaction is the only heat source, the temperature profile along the reactor should be in line with the rate of reaction. The simulated temperature profile appears physically meaningful, as the temperature rises once the reactants enter the catalytic foam and undergo an exothermic reaction. It should also be noted that the thermal-equilibrium energy transport model used in this study does not account for thermal radiation effects. The radiation effects of foam material, capillary, and the reactor wall could have an impact in the actual temperature distribution while operating in such high temperature conditions. To include the local heat transfer between strut surfaces and fluids, as well as thermal radiation effects in this CFD framework, appropriate sub-models are needed, which require further detailed studies.

It is worthwhile to highlight the lower computational costs in executing this low-dimensional CFD model. The above-mentioned results were obtained by performing simulations on one CPU (intel Core i7-8700 K) for less than half an hour. Considering the enormous effort and computational costs required for detailed simulations like strut-resolved, the results of the proposed simplified CFD approach appear promising.

Table 4
Kinetic parameters (Shishu and Kowalczyk, 1974; Sosna et al., 2020).

k[mol kg.cat^{-1} s^{-1}]	K_{CO} [Pa^{-1}]	K_{O_2} [Pa^{-1}]
$1.4\bullet10^6 e^{-45400/RT}$	$2.1\bullet10^{-5} e^{10600/RT}$	$1.3\bullet10^{-9} e^{24830/RT}$

3.2. Effect of washcoat shapes

As explained in Section 2.1.1, one of the critical parameters in defining the internal mass transport coefficient is the washcoat shape. To investigate the influence of washcoat shapes, simulations were conducted by assuming washcoat shapes of annulus and hexagon (see Table 1). For hexagonal shape, the ratio of side length to inner circle radius was assumed to be $s/R = 1.2$, with an average washcoat thickness of 5 μm. The rest of washcoat properties were kept same as in Table 3.

Fig. 4 (A) shows the comparison of CO_2 profiles for different washcoat shapes. It is inferred that the reactivity is higher while considering an annulus washcoat shape. As shown in Fig. 4 (B), the CO conversion drops by about 5 % for the hexagonal washcoat shape. The internal mass transfer coefficient is dependent on the effective diffusion length and its distribution along the fluid-washcoat interface. In the case of an annulus

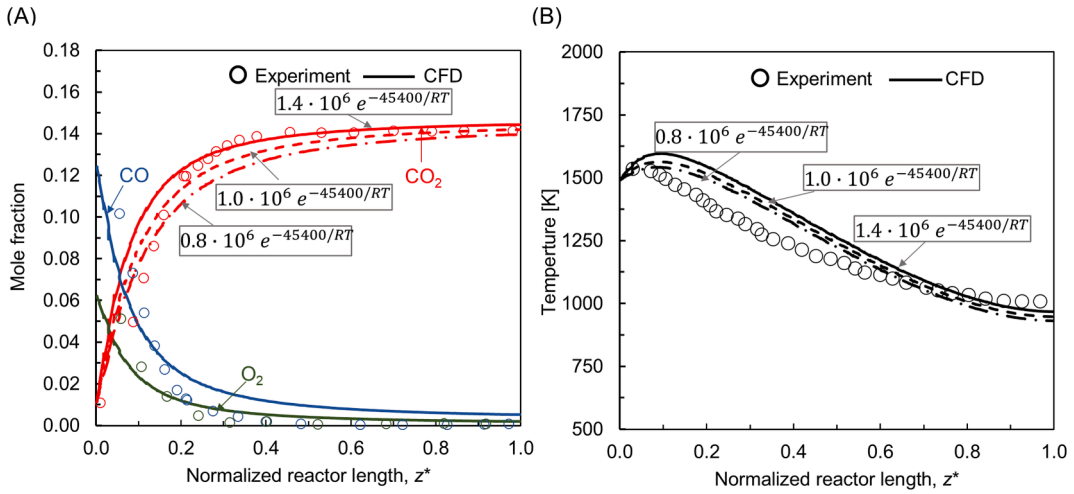

Fig. 3. Comparison of (A) species mole fraction along normalized reactor length ($z^* = z/L; L = 20.1$mm) and (B) simulated temperature profiles – Experimental data from (Dong et al., 2018) (dots) and CFD (solid lines). CO_2 and temperature profiles with dashed lines correspond to simulations with modified pre-exponential factors.

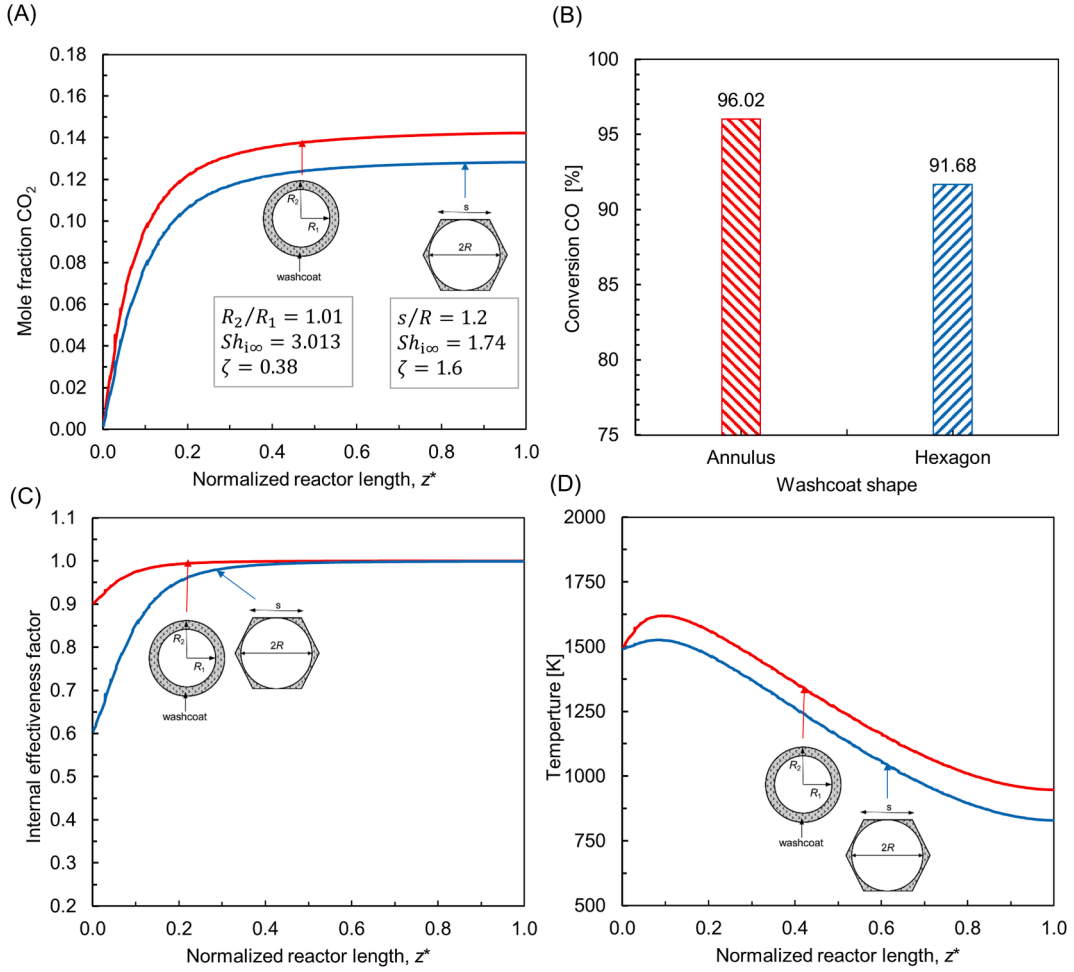

Fig. 4. Comparison of (A) CO_2 profiles along normalized reactor length ($z^* = z/L; L = 20.1$mm), (B) percentage CO conversion, (C) internal effectiveness factor (ratio of apparent reaction rate to reaction rate without washcoat diffusion resistance), and (D) axial temperature profile for different washcoat shapes (washcoat shape parameters are from ref. (Joshi et al., 2009).

shape with a uniform washcoat thickness, the spread in the diffusion length around the wetted perimeter is identical, thereby providing a similar diffusion path for all the molecules at the fluid-washcoat interface. This results in a high internal mass transfer coefficient. On the contrary, the washcoat thickness is non-uniform in the hexagonal washcoat, therefore the reacting species are subjected to different

diffusion lengths along the fluid-washcoat interface. This leads to an increase in internal mass transfer resistance. Joshi et al. (Joshi et al., 2009) have determined numerically the asymptotic Sherwood numbers for different washcoat shapes and have found that the maximum value is for the annulus shape with a uniform washcoat thickness, whereas the minimum is for hexagon. Despite this, a non-uniform catalyst distribution could yield a higher internal mass transfer coefficient, when catalysts are deposited in multiple layers and in such a way that a higher catalyst distribution is in the zone adjacent to the fluid-washcoat interface (Joshi et al., 2009). Fig. 4 (C) depicts the internal effectiveness factor, which is defined as the ratio of actual reaction rate to the reaction rate without washcoat internal diffusion resistance. It is evident that the hexagonal washcoat shape delivers lower internal effectiveness in the reaction zone due to higher internal mass transfer resistance. Fig. 4 (D) shows the axial temperature profile for different washcoat shapes. The actual reaction rate decreases for the hexagonal washcoat shape, subsequently lowering the amount of heat rejection as per Eq. (27).

3.3. Effect of washcoat thickness

The influence of washcoat thickness on mass transport is examined for 5 μm, 50 μm, and 100 μm, assuming an annulus washcoat shape, with$R_2/R_1 = 1.01$, 1.2, and 1.5, respectively. The corresponding values of $Sh_{i\infty}$ and ζ are selected from Table 1.

Fig. 5 (A) shows CO_2 profiles for different washcoat thickness. The internal mass transfer resistance increases with larger washcoat thickness, resulting in low reactivity. As shown in Fig. 5 (B), the conversion of CO drops by about 9 %, when the thickness of washcoat is increased from 5 μm to 100 μm. Increasing the washcoat thickness increases the diffusion path and makes the active catalyst sites deep within the washcoat layer less accessible, thereby reducing the internal mass transfer coefficient. At the same time, the amount of catalyst holdup decreases while the washcoat becomes thinner. Hence, it is likely that an optimum local washcoat thickness relevant to a specific reaction exists, which provides the peak conversion rate. As indicated by Fig. 5, an optimal washcoat thickness could have an axial gradient. If radial heat transfer is an issue, an optimal washcoat thickness is then a function of axial and radial reactor coordinate. Ref. (Stutz and Poulikakos, 2008) studied the optimal uniform washcoat thickness for a monolith reactor for syngas production by partial oxidation of methane and found that under the specified reaction conditions, 70 μm washcoat thickness is optimal. Fig. 5 (D) shows the comparison of internal effectiveness factor along the reactor axial direction for different washcoat thicknesses. The internal effectiveness factor is significantly reduced upon increasing the washcoat layer thickness to 100 μm due to the increased washcoat diffusion resistance. This is also reflected in the exothermicity of the reaction, as observed in axial temperature profiles in Fig. 5 (D).

3.4. Effect of washcoat tortuosity, porosity, and pore diameter

Since washcoat properties such as tortuosity, porosity, and pore diameter are difficult to quantify precisely, a certain degree of uncertainty is always inherent in them. It is therefore worthwhile to examine the influence of these washcoat parameters on the reactor performance. Fig. 6 (A, B) show the influence of different tortuosity-to-porosity ratios $\tau_{wc}/\varepsilon_{wc}$ on CO_2 profile and overall conversion, respectively. For all cases, an annulus washcoat shape with a uniform thickness of 100 μm is assumed. It is evident that the conversion decreases with an increase in $\tau_{wc}/\varepsilon_{wc}$. Higher tortuosity causes an increase in the effective diffusion length, resulting in a lower internal mass transport coefficient. On the other hand, increasing the porosity of the washcoat reduces the

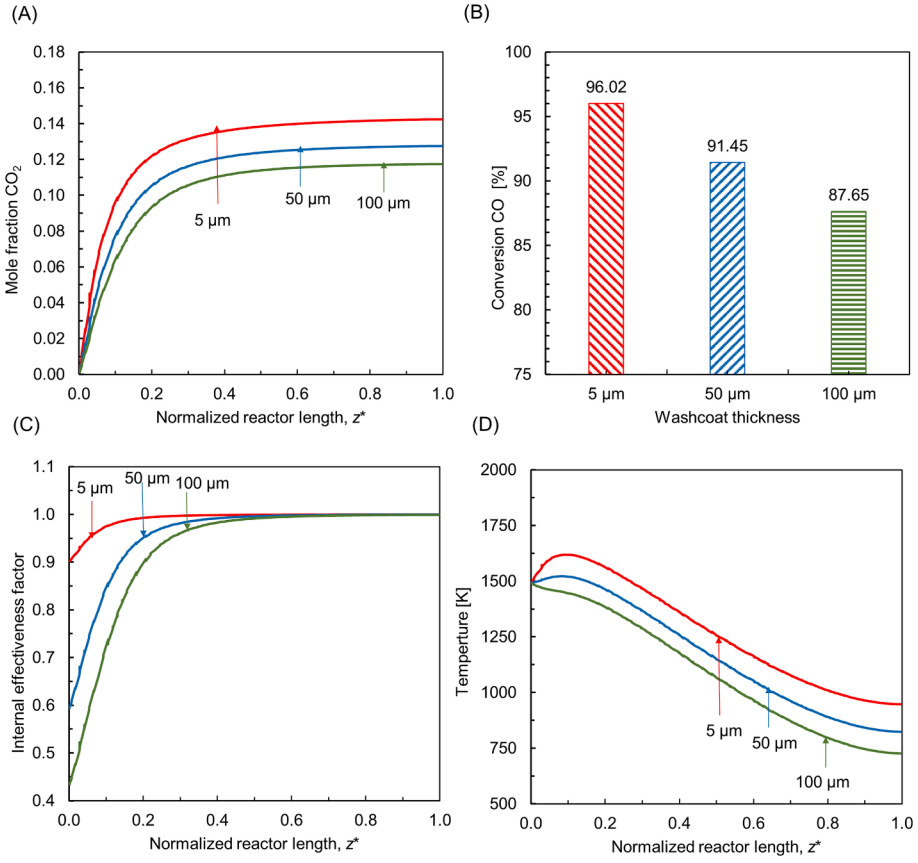

Fig. 5. Comparison of (A) CO_2 profiles along normalized reactor length ($z^* = z/L; L = 20.1$mm), (B) percentage CO conversion, (C) internal effectiveness factor (ratio of apparent reaction rate to reaction rate without washcoat diffusion resistance) and (D) axial temperature profile for different washcoat thicknesses.

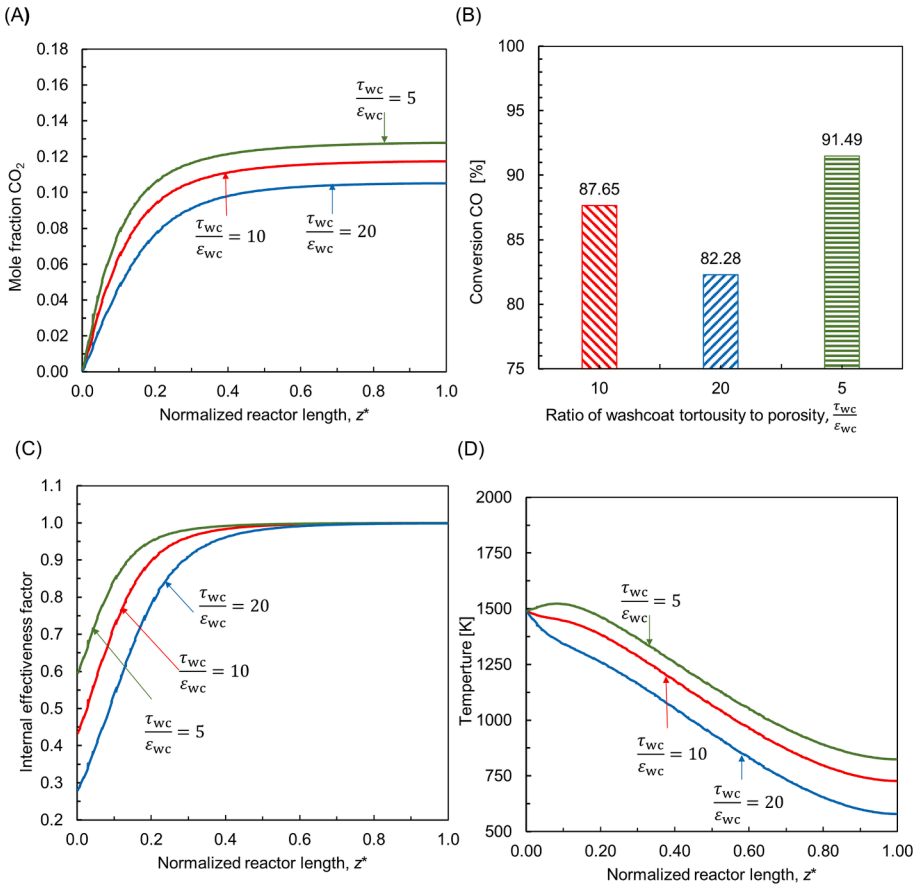

Fig. 6. Comparison of (A) CO_2 profiles along normalized reactor length ($z^* = z/L; L = 20.1$mm), (B) percentage CO conversion, (C) internal effectiveness factor (ratio of apparent reaction rate to reaction rate without washcoat diffusion resistance) and (D) axial temperature profile for different tortuosity-to-porosity ratios $\tau_{wc}/\varepsilon_{wc}$. For all cases, $d_{wc} = 10$nm.

resistance to diffusion of the reacting species into the washcoat, subsequently increasing the effective diffusion coefficient, see Eq. (11). Fig. 6 (C, D) depicts internal effectiveness factor and axial temperature profiles, respectively. The internal effectiveness factor decreases when the tortuosity-to-porosity ratio increases due to increasing washcoat diffusion resistance, which lowers the rate of reaction and exothermicity.

Fig. 7 (A-D) show the effect of washcoat average pore diameters d_{wc} on CO_2 profile, conversion, internal effectiveness factor, and axial temperature, respectively. In general, the trend in increasing the washcoat pore diameter is almost similar to the effect of decreasing the tortuosity-to-porosity ratio. With an increase in d_{wc} from 5 to 50 nm, CO conversion increases by about 15 %. The Knudsen diffusion increases with increasing d_{wc} via. Eq (10), which results in a higher effective diffusion coefficient and internal mass transfer coefficient; similar observations have been reported in ref. (von Rickenbach et al., 2015).

4. Conclusion

A simplified macroscopic CFD method is presented to model mass transport phenomena, including chemical reactions, in catalytic washcoated open-cell foams. The foam catalyst was assumed to be an isotropic porous medium, with suitable sub-models used to account for the flow resistance, species, and energy transport within the foam structure. The conversion of species during catalytic reactions was defined by the appropriate source or sink terms based on kinetic rate equations. The external and internal mass transfer resistances occurring at the fluid-washcoat interface and within the washcoat layer were considered in the species transport equations by adjusting the source terms, with the concept of external and internal Sherwood numbers taken from the literature. This enhances the flexibility of the proposed modeling approach, making it adaptable to various open-cell structures, such as periodic open-cells or gyroids. The application of such open-cell structures in the design of novel catalytic reactors has recently proven to be highly advantageous (Ambrosetti et al., 2020; Eckendörfer et al., 2024).

Catalytic CO oxidation was studied as an example. The simulated species profiles were compared with experimental data from the literature and good agreement was found for the conditions studied. Parametric studies were performed to investigate the influence of critical washcoat parameters on the proposed CFD model. The simulation results were found to be physically meaningful. By increasing the washcoat thickness and tortuosity, the internal mass transfer coefficient decreases due to a higher effective diffusion length in the washcoat. On the other hand, increasing the washcoat porosity and pore diameter allows the reactants to more easily access the washcoat catalyst layer, thus increasing the internal mass transfer coefficient.

This simplified CFD approach is particularly valuable for reactor design, such as packed beds of foam pellets or larger foam monoliths, where the internal structure of the foam cannot be resolved for cost reasons. Since the sub-models can be modified rather easily, this CFD approach can be also applied for washcoated monolith reactors. This is especially valuable, since strategies for improved catalyst design of structured reactors include double layer and zone coatings (Maurer et al., 2021; Walter et al., 2021). The proposed simplified CFD approach can support such novel catalytic reactor designs by guiding for example the preparation of porosity gradients. It should be noted that the accuracy of such lumped models is highly dependent on the reliability of the correlations used, which in turn depend on the morphological

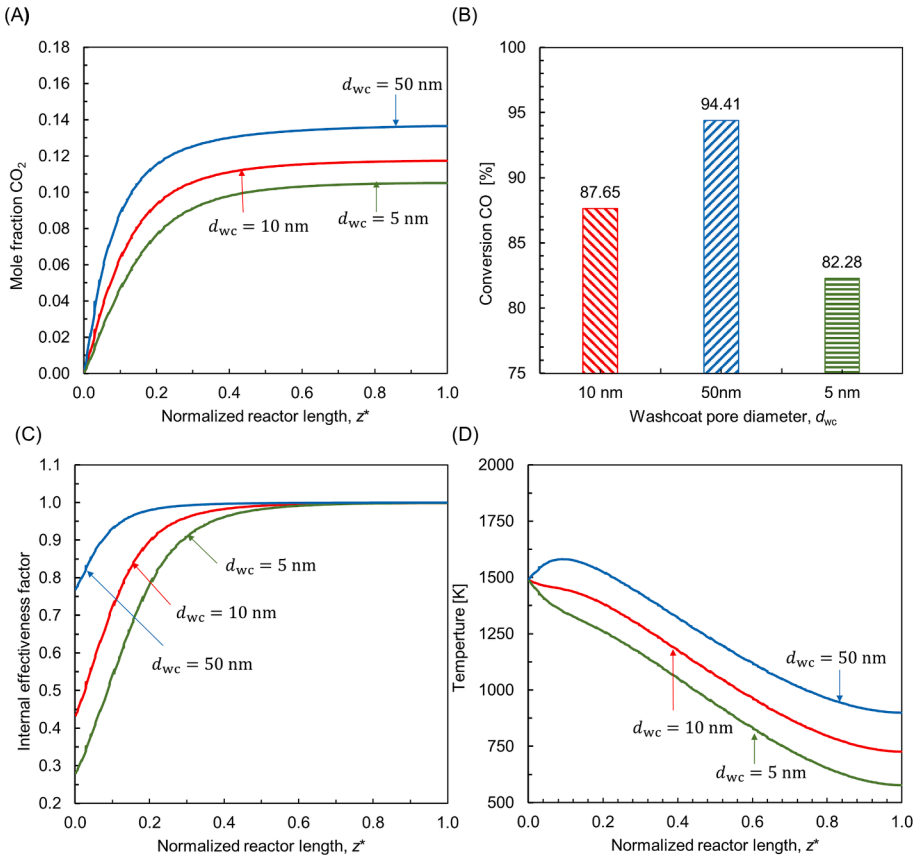

Fig. 7. Comparison of (A) CO_2 profiles along normalized reactor length ($z^* = z/L; L = 20.1$mm), (B) percentage CO conversion, (C) internal effectiveness factor (ratio of apparent reaction rate to reaction rate without washcoat diffusion resistance) and (D) axial temperature profile for different washcoat pore diameters. For all cases, $\tau_{wc}/\varepsilon_{wc} = 10$.

parameters of the foam, such as strut shape, pore size, porosity, etc. If the foam morphology deviates significantly from the typical, it would be ideal to estimate or verify the relevant correlations and foam parameters through detailed simulations using a representative volume of the foam geometry. These verified parameters can then be used as input to continuum models applied to larger reactor systems, ensuring the accuracy of the simplified model.

CRediT authorship contribution statement

Ginu R. George: Writing – review & editing, Writing – original draft, Visualization, Validation, Software, Methodology, Investigation, Formal analysis, Data curation, Conceptualization. **Sai Krishna Danda:** Software, Investigation, Data curation. **Gregor D. Wehinger:** Writing – review & editing, Writing – original draft, Supervision, Resources, Project administration, Methodology, Funding acquisition, Formal analysis, Conceptualization.

Declaration of competing interest

The authors declare that they have no known competing financial interests or personal relationships that could have appeared to influence the work reported in this paper.

Acknowledgments

G.D.W. acknowledges partial funding by Deutsche Forschungsgemeinschaft (DFG, German Research Foundation), SFB 1441, Project 426888090.

Appendix A. Supplementary data

Supplementary data to this article can be found online at https://doi.org/10.1016/j.ces.2025.121416.

Data availability

Data will be made available on request.

References

Aguirre, A., Chandra, V., Peters, E., Kuipers, J., Neira D'Angelo, M.F., 2020. Open-cell foams as catalysts support: A systematic analysis of the mass transfer limitations. Chem. Eng. J. 393, 124656. https://doi.org/10.1016/j.cej.2020.124656.

Ambrosetti, M., Groppi, G., Schwieger, W., Tronconi, E., Freund, H., 2020. Packed Periodic Open Cellular Structures – an Option for the Intensification of Non-Adiabatic Catalytic Processes. Chem. Eng. Process. 155, 108057. https://doi.org/10.1016/j.cep.2020.108057.

Balakotaiah, V., 2008. On the relationship between Aris and Sherwood numbers and friction and effectiveness factors. Chem. Eng. Sci. 63, 5802–5812. https://doi.org/10.1016/j.ces.2008.08.025.

Barteau, M.A., Ko, E.I., Madix, R.J., 1981. The oxidation of CO on the Pt(100)-(5 × 20) surface. Surf. Sci. 104, 161–180. https://doi.org/10.1016/0039-6028(81)90128-X.

Batebi, D., Abedini, R., Mosayebi, A., 2021. Kinetic Modeling of Combined Steam and CO2 Reforming of Methane over the Ni–Pd/Al2O3 Catalyst Using Langmuir–Hinshelwood and Langmuir–Freundlich Isotherms. Ind. Eng. Chem. Res. 60, 851–863. https://doi.org/10.1021/acs.iecr.0c04566.

Bhattacharya, M., Harold, M.P., Balakotaiah, V., 2004. Mass-transfer coefficients in washcoated monoliths. AIChE J 50, 2939–2955. https://doi.org/10.1002/aic.10212.

Bird, E.T., Bowden, A.E., Seeley, M.K., Fullwood, D.T., 2018. Materials selection of flexible open-cell foams in energy absorption applications. Mater. Des. 137, 414–421. https://doi.org/10.1016/j.matdes.2017.10.054.

Bracconi, M., Ambrosetti, M., Maestri, M., Groppi, G., Tronconi, E., 2018. A fundamental investigation of gas/solid mass transfer in open-cell foams using a combined experimental and CFD approach. Chem. Eng. J. 352, 558–571. https://doi.org/10.1016/j.cej.2018.07.023.

Daymo, E.A., Hettel, M., Deutschmann, O., Wehinger, G.D., 2022. Accelerating particle-resolved CFD simulations of catalytic fixed-bed reactors with DUO. Chem. Eng. Sci. 250, 117408. https://doi.org/10.1016/j.ces.2021.117408.

Della Torre, A., Lucci, F., Montenegro, G., Onorati, A., Dimopoulos Eggenschwiler, P., Tronconi, E., Groppi, G., 2016. CFD modeling of catalytic reactions in open-cell foam substrates. Comput. Chem. Eng. 92, 55–63. https://doi.org/10.1016/j.compchemeng.2016.04.031.

Deutschmann, O., Schmidt, R., Behrendt, F., Warnat, J., 1996. Numerical modeling of catalytic ignition. Symp. (Int.) Combust. 26, 1747–1754. https://doi.org/10.1016/S0082-0784(96)80400-0.

Dixon, A.G., Boudreau, J., Rocheleau, A., Troupel, A., Taskin, M.E., Nijemeisland, M., Stitt, E.H., 2012. Flow, Transport, and Reaction Interactions in Shaped Cylindrical Particles for Steam Methane Reforming. Ind. Eng. Chem. Res. 51, 15839–15854. https://doi.org/10.1021/ie202694m.

Dong, Y., Korup, O., Gerdts, J., Roldán Cuenya, B., Horn, R., 2018. Microtomography-based CFD modeling of a fixed-bed reactor with an open-cell foam monolith and experimental verification by reactor profile measurements. Chem. Eng. J. 353, 176–188. https://doi.org/10.1016/j.cej.2018.07.075.

Eckendörfer, L., Rudolf, D., Brix, A., Börnhorst, M., Freund, H., 2024. Periodic Open Cellular Structures in Chemical Engineering: Application in Catalysis and Separation Processes. Annu. Rev. Chem. Biomol. Eng. 15, 163–186. https://doi.org/10.1146/annurev-chembioeng-101121-085630.

Edouard, D., Lacroix, M., Huu, C.P., Luck, F., 2008. Pressure drop modeling on SOLID foam: State-of-the art correlation. Chem. Eng. J. 144, 299–311. https://doi.org/10.1016/j.cej.2008.06.007.

Ferziger, J.H., Perić, M., 2002. Computational Methods for Fluid Dynamics. Springer, Berlin Heidelberg, Berlin, Heidelberg.

S. Fogler, Elements of Chemical Reaction Engineering, sixth ed., Pearson, 2020.

George, G.R., Bockelmann, M., Schmalhorst, L., Beton, D., Gerstle, A., Torkuhl, L., Lindermeir, A., Wehinger, G.D., 2021. Workflow for computational fluid dynamics modeling of fixed-bed reactors packed with metal foam pellets: Hydrodynamics. AIChE J 46, 559. https://doi.org/10.1002/aic.17284.

George, G.R., Bockelmann, M., Schmalhorst, L., Beton, D., Gerstle, A., Lindermeir, A., Wehinger, G.D., 2022. Radial heat transport in a fixed-bed reactor made of metallic foam pellets: Experiment and particle-resolved computational fluid dynamics. Int. J. Heat Mass Transf. 197, 123376. https://doi.org/10.1016/j.ijheatmasstransfer.2022.123376.

George, G.R., Bockelmann, M., Schmalhorst, L., Beton, D., Gerstle, A., Lindermeir, A., Wehinger, G.D., 2023. Optimization of metal foam pellet shape in packed beds for improved radial heat transfer using particle-resolved computational fluid dynamics. Chem. Eng. Process. 188, 109357. https://doi.org/10.1016/j.cep.2023.109357.

Giani, L., Groppi, G., Tronconi, E., 2005. Heat Transfer Characterization of Metallic Foams. Ind. Eng. Chem. Res. 44, 9078–9085. https://doi.org/10.1021/ie050598p.

Giani, L., Groppi, G., Tronconi, E., 2005. Mass-Transfer Characterization of Metallic Foams as Supports for Structured Catalysts. Ind. Eng. Chem. Res. 44, 4993–5002. https://doi.org/10.1021/ie0490886.

Groppi, G., Giani, L., Tronconi, E., 2007. Generalized correlation for gas/solid mass-transfer coefficients in metallic and ceramic foams. Ind. Eng. Chem. Res. 46, 3955–3958. https://doi.org/10.1021/ie061330g.

Hayes, R.E., Fadic, A., Mmbaga, J., Najafi, A., 2012. CFD modelling of the automotive catalytic converter. Catal. Today 188, 94–105. https://doi.org/10.1016/j.cattod.2012.03.015.

Ho, P.H., de Nolf, W., Ospitali, F., Beton, D., Torkuhl, L., Fornasari, G., Vaccari, A., Benito, P., 2019. Insights into coated NiCrAl open-cell foams for the catalytic partial oxidation of CH 4. React. Chem. Eng. 4, 1768–1778. https://doi.org/10.1039/C9RE00178F.

Hou, K., Hughes, R., 2001. The kinetics of methane steam reforming over a Ni/α-Al2O catalyst. Chem. Eng. J. 82, 311–328. https://doi.org/10.1016/S1385-8947(00)00367-3.

Inayat, A., 2013. Open-cell Foams as Catalyst Support: A Description of Morphology, Fluid Dynamics and Catalytic Performance: Offenzellige Schäume als Katalysatorträger: Beschreibung von Morphologie. Fluiddynamik und katalytischer Performance, PhD.

Inayat, A., Klumpp, M., Lämmermann, M., Freund, H., Schwieger, W., 2016. Development of a new pressure drop correlation for open-cell foams based completely on theoretical grounds: Taking into account strut shape and geometric tortuosity. Chem. Eng. J. 287, 704–719. https://doi.org/10.1016/j.cej.2015.11.050.

Incera Garrido, G., Kraushaar-Czarnetzki, B., 2010. A general correlation for mass transfer in isotropic and anisotropic solid foams. Chem. Eng. Sci. 65, 2255–2257. https://doi.org/10.1016/j.ces.2009.12.016.

Incera Garrido, G., Patcas, F.C., Lang, S., Kraushaar-Czarnetzki, B., 2008. Mass transfer and pressure drop in ceramic foams: A description for different pore sizes and porosities. Chem. Eng. Sci. 63, 5202–5217. https://doi.org/10.1016/j.ces.2008.06.015.

Incropera, F.P., DeWitt, D.P., Bergman, T.L., Lavine, A.S., 2007. Fundamentals of heat and mass transfer, sixth ed. Wiley, Hoboken, NJ.

Joshi, S.Y., Harold, M.P., Balakotaiah, V., 2009. On the use of internal mass transfer coefficients in modeling of diffusion and reaction in catalytic monoliths. Chem. Eng. Sci. 64, 4976–4991. https://doi.org/10.1016/j.ces.2009.08.008.

Joshi, S.Y., Harold, M.P., Balakotaiah, V., 2009. Low-dimensional models for real time simulations of catalytic monoliths. AIChE J 55, 1771–1783. https://doi.org/10.1002/aic.11794.

Karthik, G.M., Buwa, V.V., 2017. Effect of particle shape on fluid flow and heat transfer for methane steam reforming reactions in a packed bed. AIChE J 63, 366–377. https://doi.org/10.1002/aic.15542.

Kim, S., Lee, C.-W., 2014. A review on manufacturing and application of open-cell metal foam. Procedia Mater. Sci. 4, 305–309. https://doi.org/10.1016/j.mspro.2014.07.562.

Korup, O., Mavlyankariev, S., Geske, M., Goldsmith, C.F., Horn, R., 2011. Measurement and analysis of spatial reactor profiles in high temperature catalysis research. Chem. Eng. Process. 50, 998–1009. https://doi.org/10.1016/j.cep.2011.05.024.

Kumar, P., Topin, F., 2017. State-of-the-art of pressure drop in open-cell porous foams: review of experiments and correlations. J. Fluids Eng. 139, 5202. https://doi.org/10.1115/1.4037034.

Lacroix, M., Nguyen, P., Schweich, D., Pham Huu, C., Savin-Poncet, S., Edouard, D., 2007. Pressure drop measurements and modeling on SiC foams. Chem. Eng. Sci. 62, 3259–3267. https://doi.org/10.1016/j.ces.2007.03.027.

Lu, T.J., Stone, H.A., Ashby, M.F., 1998. Heat transfer in open-cell metal foams. Acta Mater. 46, 3619–3635. https://doi.org/10.1016/S1359-6454(98)00031-7.

Maestri, M., Cuoci, A., 2013. Coupling CFD with detailed microkinetic modeling in heterogeneous catalysis. Chem. Eng. Sci. 96, 106–117. https://doi.org/10.1016/j.ces.2013.03.048.

Makhania, M., Upadhyayula, S., 2022. Foam: Imparting Structure to Heterogeneous Catalysis. ChemBioEng Rev. 46, 4166. https://doi.org/10.1002/cben.202200007.

Makhania, M., Upadhyayula, S., 2022. Diffusion and reaction in foam-based catalysts: Identifying the shape factor. Chem. Eng. Sci. 250, 117381. https://doi.org/10.1016/j.ces.2021.117381.

Manetti, L.L., de Oliveira, I.L., Cardoso, E.M., 2022. Thermal efficiency of open-cell metal foams: Impact of foam thickness by comparing correlations and numerical modeling. Appl. Therm. Eng. 207, 118219. https://doi.org/10.1016/j.applthermaleng.2022.118219.

Maurer, F., Gänzler, A., Lott, P., Betz, B., Votsmeier, M., Loridant, S., Vernoux, P., Murzin, V., Bornmann, B., Frahm, R., Deutschmann, O., Casapu, M., Grunwaldt, J.-D., 2021. Spatiotemporal Investigation of the Temperature and Structure of a Pt/CeO2 Oxidation Catalyst for CO and Hydrocarbon Oxidation during Pulse Activation. Ind. Eng. Chem. Res. 60, 6662–6675. https://doi.org/10.1021/acs.iecr.0c05798.

Moncada Quintero, C.W., Ercolino, G., Poozhikunnath, A., Maric, R., Specchia, S., 2021. Analysis of heat and mass transfer limitations for the combustion of methane emissions on PdO/Co3O4 coated on ceramic open cell foams. Chem. Eng. J. 405, 126970. https://doi.org/10.1016/j.cej.2020.126970.

Napolitano, M., Romano, R., Dragonetti, R., 2017. Open-cell foams for thermoacoustic applications. Energy 138, 147–156. https://doi.org/10.1016/j.energy.2017.07.042.

Ozmat, B., Leyda, B., Benson, B., 2004. Thermal Applications of Open-Cell Metal Foams. Mater. Manuf. Process. 19, 839–862. https://doi.org/10.1081/AMP-200030568.

Papetti, V., Dimopoulos Eggenschwiler, P., Della Torre, A., Lucci, F., Ortona, A., Montenegro, G., 2018. Additive Manufactured open cell polyhedral structures as substrates for automotive catalysts. Int. J. Heat Mass Transfer 126, 1035–1047. https://doi.org/10.1016/j.ijheatmasstransfer.2018.06.061.

Patcas, F.C., Garrido, G.I., Kraushaar-Czarnetzki, B., 2007. CO oxidation over structured carriers: A comparison of ceramic foams, honeycombs and beads. Chem. Eng. Sci. 62, 3984–3990. https://doi.org/10.1016/j.ces.2007.04.039.

Roy, S., Heibel, A.K., Liu, W., Boger, T., 2004. Design of monolithic catalysts for multiphase reactions. Chem. Eng. Sci. 59, 957–966. https://doi.org/10.1016/j.ces.2003.12.001.

Schuetz, M., Glicksman, L., 1984. A basic study of heat transfer through foam insulation. J. Cell. Plast. March-April 114–121.

Shishu, R., Kowalczyk, L., 1974. The Oxidation of Carbon Monoxide on Supported Platinum A Study of Honeycomb Catalyst Reaction Kinetics. Platin. Met. Rev. 18, 58–64.

Siemens Digital Industries Software, Simcenter STAR-CCM+User Guide, version 2020.1, Siemens, 2020.

Sosna, B., Korup, O., Horn, R., 2020. Probing local diffusion and reaction in a porous catalyst pellet. J. Catal. 381, 285–294. https://doi.org/10.1016/j.jcat.2019.11.005.

Stutz, M.J., Poulikakos, D., 2008. Optimum washcoat thickness of a monolith reactor for syngas production by partial oxidation of methane. Chem. Eng. Sci. 63, 1761–1770. https://doi.org/10.1016/j.ces.2007.11.032.

Twigg, M.V., Richardson, J.T., 2007. Fundamentals and Applications of Structured Ceramic Foam Catalysts. Ind. Eng. Chem. Res. 46, 4166–4177. https://doi.org/10.1021/ie061122o.

Versteeg, H.K., Malalasekera, W. 2007. An introduction to computational fluid dynamics: The finite volume method / H.K. Versteeg and W. Malalasekera, secondnd ed., Pearson Education, Harlow, Essex.

von Rickenbach, J., Lucci, F., Narayanan, C., Dimopoulos Eggenschwiler, P., Poulikakos, D., 2015. Effect of washcoat diffusion resistance in foam based catalytic reactors. Chem. Eng. J. 276, 388–397. https://doi.org/10.1016/j.cej.2015.03.132.

Walter, R., Neumann, J., Hinrichsen, O., 2021. Modeling the Catalytic Performance of Coated Gasoline Particulate Filters under Various Operating Conditions. Ind. Eng. Chem. Res. 60, 16993–17005. https://doi.org/10.1021/acs.iecr.1c03631.

Walther, G., Klöden, B., Büttner, T., Weißgärber, T., Kieback, B., Böhm, A., Naumann, D., Saberi, S., Timberg, L., 2008. A New Class of High Temperature and Corrosion Resistant Nickel-Based Open-Cell Foams. Adv. Eng. Mater. 10, 803–811. https://doi.org/10.1002/adem.200800088.

Wan, T., Liu, Y., Zhou, C., Chen, X., Li, Y., 2021. Fabrication, properties, and applications of open-cell aluminum foams: A review. J. Mater. Sci. Technol. 62, 11–24. https://doi.org/10.1016/j.jmst.2020.05.039.

Wang, H., Guo, L., Chen, K., 2020. Theoretical and experimental advances on heat transfer and flow characteristics of metal foams. Sci. China Technol. Sci. 63, 705–718. https://doi.org/10.1007/s11431-019-1455-0.

Wehinger, G.D., Heitmann, H., Kraume, M., 2016. An artificial structure modeler for 3D CFD simulations of catalytic foams. Chem. Eng. J. 284, 543–556. https://doi.org/10.1016/j.cej.2015.09.014.

Zhao, C.Y., 2012. Review on thermal transport in high porosity cellular metal foams with open cells. Int. J. Heat Mass Transf. 55, 3618–3632. https://doi.org/10.1016/j.ijheatmasstransfer.2012.03.017.